The effect of heat treatment on the microstructure and mechanical properties of 3D-printed AlSi9Cu3Fe alloy

M Roudnicka[1,2], D Dvorsky[1,2] and D Vojtech[1]

[1]Department of Metals and Corrosion Engineering, University of Chemistry and technology Prague, Technicka 5, 166 28 Prague 6, Czech Republic

[2]Institute of Physics, Academy of Sciences of the Czech Republic (AS CR), Na Slovance 1999/2, 182 21 Prague 8, Czech Republic

E-mail: michaela.roudnicka@vscht.cz

Abstract. In this paper, we characterize AlSi9Cu3Fe alloy prepared by selective laser melting (SLM); a 3D printing technique based on the localized melting of a powder material by a laser beam in thin successively deposited layers. The layer-wise building-up resulted in an anisotropic and hierarchical microstructure of this alloy. High cooling rates brought a very fine microstructure, which contributed to high material strength, but also residual stresses, which are undesirable. Residual stresses can be reduced by various heat treatments. We carried out stress-relief and T6 heat treatments and studied their effect on the microstructure and mechanical properties. T6 heat treatment brought a significant increase in tensile yield strength.

1 Introduction

Al–Si–Cu alloys have been employed for various engineering applications due to their low density and good strength, especially for replacement of cast iron and steels in automobile parts [1]. Alloys based on Al-Si system are well known for their good castability due to eutectic transformation. However, conventional manufacturing via casting, working and welding is limited in terms of component geometry. A possible solution for the production of complex parts is the application of additive manufacturing (AM) technologies.

Due to processing materials layer upon layer by localized heat source, additively manufactured parts have usually different features from traditionally produced parts. Between irradiated volume and its surroundings, there are great temperature gradients. Melt pools thus solidify under cooling rates reaching up to 10^6 °C/s [2]. Under such rates, microstructure evolution can become completely distinctive. Generally, very fine microstructures are obtained [3] but phase composition and other microstructural features can vary depending on specific materials and specific processing conditions.

Selective Laser Melting (SLM) is one of the most promising AM techniques. Although it is one of the most thoroughly studied and advanced techniques, there are some weak sides we have to deal with. Because SLM belongs among powder-bed techniques, SLM parts suffers poor surface quality as particles of surrounding loose powder adhere to their surface. Therefore, even though SLM enables direct production of net parts, some additional treatment is often required to obtain high-quality surface. Otherwise, high surface roughness strongly limits material fatigue life [4]. Another

weak side of SLM manufactured metals is often their low plasticity. Due to steep temperature gradients (10^4 °C/mm) in melt pools, large thermal stresses remain in materials [5].
Retained internal stresses can be minimized already before actual production by setting of the SLM process. The first step is to select an appropriate scanning strategy. Osakada and Shiomi [6] concluded that the thermal stress increase with longer laser distance. Therefore, it is advisable to build parts in segments (e.g. chess-board scanning strategy). Mercelis et al. [7] also found that stresses are higher in the building direction than in the perpendicular one and so residual stresses increase with the height of SLM parts. Hence, orientation of parts can be considered before production too. In some SLM machines that enable preheating of the substrate, temperature gradients can be lowered and so the residual stresses, however, at the expense of yield strength [8].
After the manufacture, residual stresses can be reduced by heat treatment. Before the removal from the build substrate, most SLM producers recommend to subject final parts to a so-called stress-relief treatment to avoid possible deformations [7, 9]. For example, material data sheets for AlSi10Mg alloy by EOS or Renishaw suggest 300 °C/2 h. Another possibility is to apply different modes of heat treatment and tune microstructures and mechanical properties according to requirements given by a particular application. T6 heat treatment is commonly used to increase the strength of conventionally manufactured Al-Si alloys containing Cu or Mg. During solution treatment at a higher temperature, large intermetallic particles dissolve and alloying elements redistribute homogeneously. During artificial aging at a lower temperature fine precipitates are formed [10]. When the material is loaded, these homogeneously distributed precipitates become efficient obstacles for dislocation movement. For the here-studied AlSi9Cu3Fe alloy containing 3 wt.% of copper, T6 heat treatment might be thus applied to induce precipitation strengthening by Cu-rich precipitates [11].
So far, there are not many references in the literature to the preparation and characterization of AlSi9Cu3Fe alloy by AM. Therefore, we studied and characterized this alloy prepared by SLM. We subjected it to two conventional heat treatments – stress-relief and T6 - and described their effect on microstructural changes and mechanical properties.

2 Materials and Methods

2.1 Specimens preparation

Samples of AlSi9Cu3Fe alloy (chemical composition given in table 1) were prepared by means of metallic 3D printing by NETME Centre in Brno. Selective laser melting (SLM) technology was applied (SLM Solution 280HL machine). Fine gas-atomized powder of AlSi9Cu3Fe alloy (LPW, $d_{average}$ = 40 μm) was compacted by localized melting of a 400W laser beam. The laser beam melted the powder material, deposited in 50 μm thin layers, according to a chess board scanning strategy, with a hatching distance between adjacent scan lines set to 150 μm. The scanning speed of the laser beam was 1300 mm/s. The working chamber was supplied with an argon atmosphere to prevent the powder oxidation.

Table 1. Chemical composition of the SLM AlSi9Cu3Fe alloy.

wt.%	**Al**	**Si**	**Cu**	**Fe**	**Mg**	**Zn**	**P**
SLM	bal.	8.9±0.1	3.1±0.1	1.2±0.1	0.3±0.02	0.01	0.01

SLM provided a set of samples intended for mechanical testing, directly in the form given by the input 3D CAD model (dog-bone samples). All samples were printed in vertical orientation. As their surface was covered with adherent particles of surrounding powder, sand-blasting was applied to smoothen the surface.
One third of the tested samples was kept in the as-built form. The rest of the samples were subjected to heat treatment (HT) in a muffle furnace Martinek MP 05. Two common HT regimes were applied: (1) stress-relief HT to remove residual stresses, and (2) T6 HT to induce precipitation of θ″ hardening phase. Stress-relief HT was carried out at a temperature of 300 °C for 2 hours. For

T6 HT, samples were solution treated at 520 °C/6 h, water-quenched and artificially aged at 160 °C/10 h.

2.2 Characterization of microstructural changes

For each material state (as-built, stress-relieved, T6), microstructure was studied on longitudinal metallographic sections. After etching in 5% HF, microstructures were observed by light metallographic microscope OLYMPUS PME 3 and scanning electron microscope TESCAN VEGA-3 LMU. Scanning electron microscopy (SEM) was completed by EDS analysis (Oxford instruments INCA 350 analyzer). Phase composition was determined by X-ray diffraction (XRD, PANalytical X'Pert PRO with Cu anode, High Score Plus software).

2.3 Mechanical testing

On the prepared metallographic section, Vicker's hardness HV1 (1 kg load, 10 s persistence) was measured using a Future-Tech FM-700 microhardness tester. Average hardness was evaluated statistically from 10 measurements. Uniaxial tensile tests were carried out on a universal loading machine LabTest 250SP1- VM. All measurements were carried out under a constant deformation rate of 0.001 s^{-1}.

3 Results and Discussion

3.1 Microstructure of 3D-printed AlSi9Cu3Fe alloy

Gradual localized melting of powder material repeatedly in many successive layers is responsible for the formation of distinctive microstructure of the AlSi9Cu3Fe alloy. At the moment when the beam is focused on powder layer (interaction time in ms), it melts a certain volume of the material. As the beam is moved away in its vector, the melt solidifies. As a result, we can observe solidified melt pools in the microstructure (figure 1a-b). Their width and depth reaches about 200-250 μm, which approximately corresponds to the size of the laser beam spot. The depth of melt pools exceeds the thickness of a powder layer by a factor of 4-5, which is important for ensuring good interconnection between layers.

In higher magnification, one can see that the microstructure is formed by very fine cellular substructure (figure 1c-d). Inside melt pools, cells are finer (figure 1c) and elongated in one direction. Their width and length was determined by image analysis as 1.0±0.1 μm and 3.7±0.8 μm, respectively. Such fineness is the result of very high cooling rates [2]. The elongation and directionality of cells is determined by temperature gradients in melt pools. From the hottest center of a melt pool, the heat is radially conducted away by already solidified material or surrounding powder. Because cellular substructure is very homogeneous in the whole material, it is hard to distinguish grains. Nevertheless, slight differences in cell morphologies and optical contrast between particular grains make it possible to discern columnar grains growing from pool borders towards their centers (indicated by dashed lines in figure 1b). At melt pool borders, cells are larger and more rounded (figure 1d), which is caused by lower undercooling at the interface between a melt pool and its surroundings [12].

Comparable to AlSi10Mg alloy prepared by SLM [13, 14], in AlSi9Cu3Fe alloy, the intercellular network is formed by eutectic Si and the cells by oversaturated solid solution α-Al. EDS quantified the chemical composition of the solid solution and showed 5.4±0.5 wt.% of Si, 3.2±0.4 wt.% of Cu and 1.1±0.2 wt.% of Fe. However, the quantification is distorted by surrounding Si network which interferes with the interaction volume of the EDS analysis. Therefore, it can be expected that the actual content of Si in the solid solution is lower. Further measurement in transmission mode of electron microscopy is planned to obtain more accurate evaluation. Except from the two main constituting components, XRD also revealed the presence of small amount of Al_2Cu phase (2 vol.%).

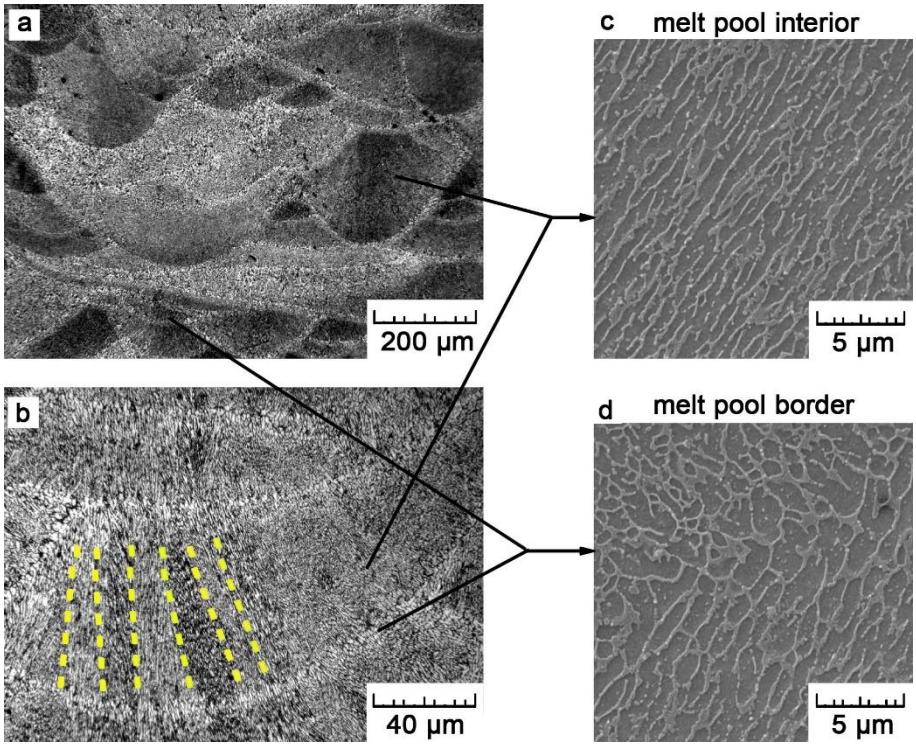

Figure 1. Microstructure of the SLM AlSi9Cu3Fe alloy: (a) melt pools, (b) melt pool interiors (dashed lines indicate grains), (c) cellular structure inside melt pools and (d) cellular structure at melt pool borders.

3.2 Microstructural changes after heat treatment

Microstructural changes after applied heat treatments are depicted by micrographs in figure 2. Microstructure after stress-relief HT (figure 2b,e) does not apparently differ from the as-built microstructure (figure 2a,d). Only slight coarsening of Si network and its initial disruption into idiomorphic particles was observed. Increased temperature enhanced Si diffusion from the oversaturated solid solution. Otherwise, additively built macrostructure remained unchanged. After T6 HT, microstructure homogenized (figure 2c,f); melt pool borders vanished and the Si network completely disintegrated. High temperatures during solution treatment led to Si diffusion and formation of large Si particles (1-3 µm in diameter). Also, needlelike Al_5FeSi phase formed (figure 2f). Subsequent quenching again resulted in an oversaturated solid solution α(Al)′ with concentrations of alloying elements higher than their maximal equilibrium solubility. Therefore, at subsequent aging, oversaturated solid solution α(Al)′ decomposed into coherent GP zones followed by precipitation of fine θ″ phases. Within the scope of this work, it was not possible to visualize the precipitates but their presence is highly anticipated as the course of T6 heat treatment is the same as for castings [15]. In Al-Si-Cu alloys, GP zones consisting of localized concentrations of Cu atoms form at room temperature already. Above 100 °C, GP zones dissolve and are replaced by θ″ phases. With longer aging time, θ″ phase transforms into the metastable θ′ semi-coherent with the matrix. Finally the stable incoherent equilibrium phase θ (Al_2Cu) is formed. Maximum strength is obtained when the highest fraction of θ″ phase is present [10].

By comparison of images a-c in figure 2, it is apparent that a significant amount of small pores appeared after T6 HT. Most probably, the porosity formed due to the melting of Al_2Cu phase during solution treatment at 520 °C. By image analysis, the porosity was assessed to represent 2 vol.%, which corresponds to the amount of Al_2Cu phase detected in the material in the as-built state. For Al-Si-Cu alloys, there is a risk of the incipient melting of Cu-rich phases at temperatures higher than 495˚C. On the other hand, solution treatment at temperatures of 495˚C or less is not capable of maximizing the dissolution of the copper-rich phases, nor is it able to modify the silicon

particle morphology sufficiently [16]. Gautier et al. [17] showed that the best combination of tensile strength and ductility is obtained with solution treatment at 515°C.

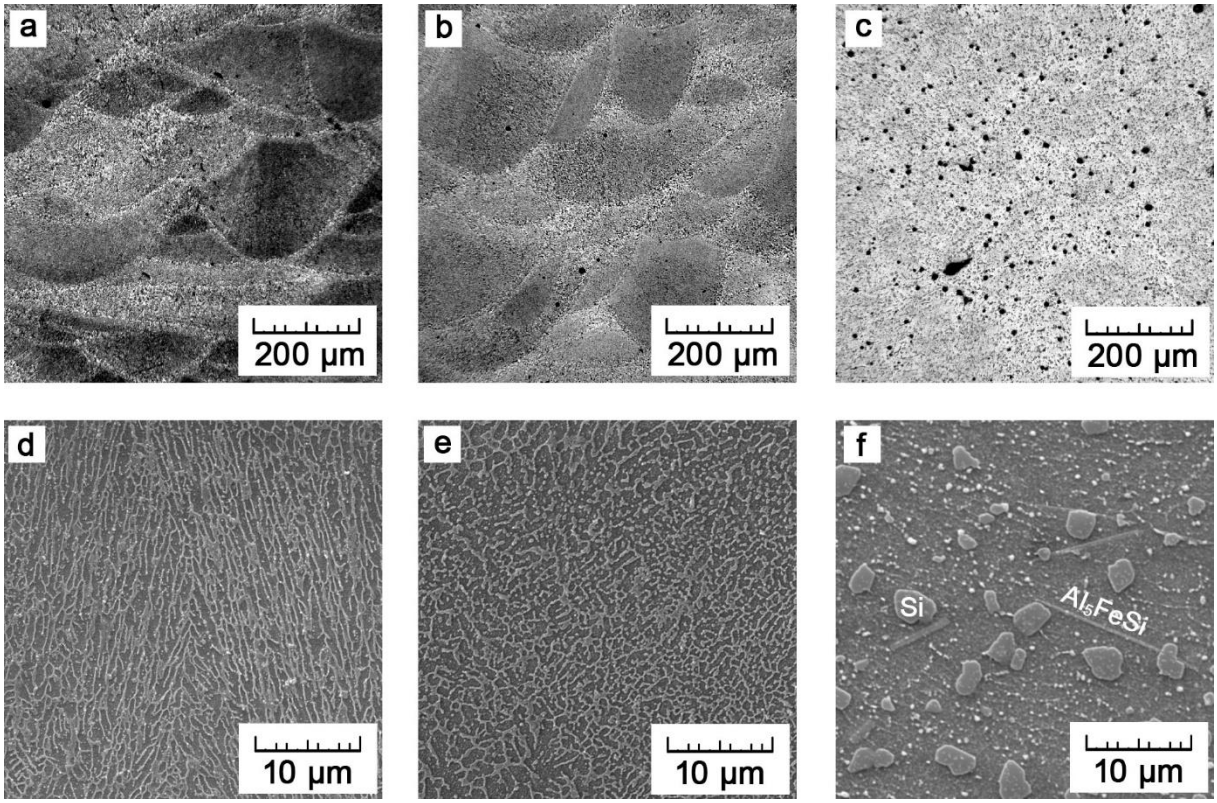

Figure 2. Microstructures of the SLM AlSi9Cu3Fe alloy: (a,d) as-built, (b,e) stress-relieved and (c,f) T6.

3.3 Mechanical properties

Changes in mechanical properties related to heat treatment are described by chart in figure 3.

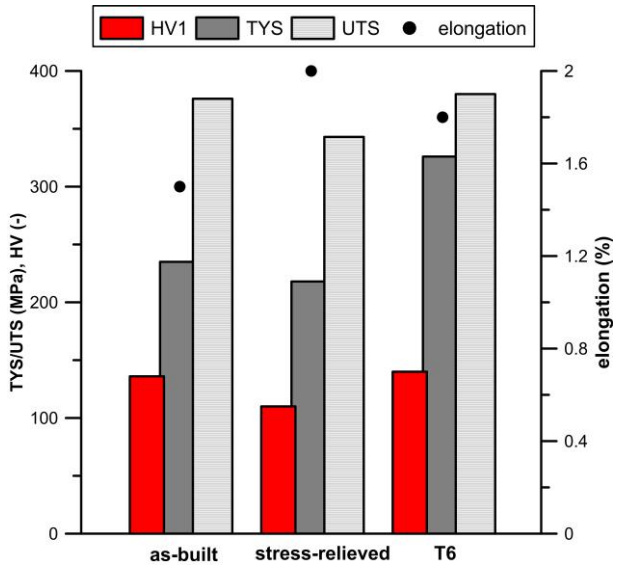

Figure 3. Changes of mechanical properties of the SLM AlSi9Cu3Fe alloy after heat treatment.

Vickers hardness do not show significant differences. Stress-relief HT relieved residual stresses and subtly coarsened the Si network, which resulted in a slight decrease in hardness (from 136±4 to 110±3 HV1). After T6 HT, hardness remained almost unchanged. Hardening brought by precipitation of θ″ phase was counterweighted by softening due to the break-up of Si network forming fine cellular microstructure and significant coarsening of Si particles. Ultimate tensile strengths (UTS) show a similar trend. In addition to the described features, the increase in UTS in T6 condition was also limited by porosity.

The effect of precipitation strengthening by θ″ phase is more pronounced in the values of tensile yield strength (TYS). After T6 HT, about 40% increase in TYS was registered. Elongation remained at a comparable level. Negative effects of precipitation strengthening, brittle Al_5FeSi phase and porosity on elongation were offset by an increase in plasticity due to the break-up of Si network.

Compared to SLM-fabricated AlSi10Mg alloys, where the T6 HT resulted in decrease in tensile strength due to the coarsening of Si precipitates [12, 13], in AlSi9Cu3Fe alloy, this treatment have shown to be contributory in terms of TYS.

4 Conclusion

Two heat treatments of the AlSi9Cu3Fe alloy prepared by 3D printing technique SLM have been studied. Stress-relief did not significantly change the microstructure, only relieved residual stresses resulting from high cooling rates during SLM. After T6 heat treatment, characteristic 3D-printed microstructure completely vanished. During solution treatment and subsequent quenching, fine cellular substructure disintegrated and Si and Al_5FeSi phases formed in the matrix of oversaturated α(Al)′ solid solution. Aging led to the precipitation of fine θ″ precipitates, bringing a significant increase in tensile yield strength.

Acknowledgements

Authors wish to thank the Czech Science Foundation (project no. P108/12/G043) and specific university research (MSMT No 21-SVV/2018) for the financial support of this research.

References

[1] Okayasu M, Takeuchi S and Ochi T 2017 *Int. J. Cast Metals Res.* **30** 217-225
[2] Brandl E, Heckenberger U, Holzinger V and Buchbinder D 2012 *Mater. Design* **34** 159-169
[3] Wang L Z, Wu J J, Huang X F and Hong X F 2018 *Opt. Laser Technol.* **107** 89-98
[4] Olakanmi E O 2013 *J. Mater. Process. Technol.* **213** 1387-1405
[5] Li Y and Gu D 2014 *Addit. Manuf.* **1-4** 99-109
[6] Osakada K and Shiomi M 2006 *Int. J. Mach. Tools Manuf.* **46** 1188-1193
[7] Peter M and Jean-Pierre K 2006 *Rapid Prototyp. J.* **12** 254-265
[8] Buchbinder D, Meiners W, Pirch N, Wissenbach K and Schrage J 2014 *J. Laser Appl.* **26** 012004
[9] Sun S, Brandt M and Easton M 2017 Laser Additive Manufacturing: Materials, Design, Technologies and Applications ed M. Brandt (Cambridge: Woodhead Publishing) chapter 2 p 55-77
[10] Sjölander E and Seifeddine S 2010 *J. Mater. Process. Technol.* **210** 1249-1259
[11] Mondolfo L F 1976 Aluminum alloys: structure and properties (London: Butterworths)
[12] Li W, Li S, Liu J, Zhang A, Zhou Y, Wei Q, Yan C and Shi Y 2016 *Mater. Sci. Eng. A* **663** 116-125
[13] Fousova M, Dvorsky D, Michalcova A and Vojtech D 2018 *Mater. Charact.* **137** 119-126
[14] Zhou L, Mehta A, Schulz E, McWilliams B, Cho K and Sohn Y 2018 *Mater. Charact.* in press
[15] Kang H, Kida M, Miyahara H and Ogi K 1997 *J. JFS* **69** 828-834
[16] Samuel A M, Doty H W, Valtierra S and Samuel F H 2013 *Int. J. Cast Metals Res* **26** 354-363
[17] Gauthier J, Louchez P and Samuel F 1995 *Cast Metals* **8** 91-106